Lab on a Chip

PAPER

Controlling uniformity of photopolymerized microscopic hydrogels†

Cite this: *Lab Chip*, 2014, **14**, 1551

Sukho Park,[ab] Dongshin Kim,[b] Seong Young Ko,[a] Jong-Oh Park,[a] Sathish Akella,[b] Bing Xu,[c] Ye Zhang[c] and Seth Fraden*[b]

Received 5th February 2014,
Accepted 7th February 2014

DOI: 10.1039/c4lc00158c

www.rsc.org/loc

This paper studies hydrogels created by photopolymerization with a uniform beam of light. Under some conditions the density profiles of the resulting hydrogels were uniform cylinders, mirroring the illumination profiles. However, under other conditions, gels with hollow cylindrical shapes were formed. We studied the photopolymerization of poly-*N*-isopropylacrylamide (pNIPAAM), a hydrogel that has been widely used in tissue engineering and microfluidic applications, and examined how the size and uniformity of pNIPAAM microscopic gels can be controlled by varying parameters such as exposure time, exposure area, exposure intensity, monomer concentration, photoinitiator concentration and terminator concentration. A simplified reaction–diffusion model of the polymerization process was developed and was found to describe the experiment for a wide range of parameters. This general framework will guide attempts to establish optimal conditions for the construction of microscopic hydrogels using photolithography, which is a method that has found applications in fields such as microfluidics, drug delivery, cell and tissue culturing, and high resolution 3D printing.

1. Introduction

This paper is concerned with photopolymerization of patterned hydrogels on the length scale of tens to hundreds of microns. Photopolymerization methods, illustrated in Fig. 1, are divided into two classes: printing with masks and direct writing. The latter category is further subdivided into two methods: digital projection and laser scanning.[1] Common to the successful application of all photopolymerization methods is the assumption that the pattern of the photopolymerized gel will mimic the pattern of illumination. Indeed, when this assumption breaks down it becomes very difficult to pattern hydrogels on the microscale. In nearly all photopolymerization studies reported to date, the patterned gels have reflected the illumination pattern. Here we present the surprising evidence of non-uniform gels formed with uniform illumination and develop a general theory that differentiates those conditions under which uniform illumination produces uniform gels from those conditions that do not. Furthermore, our work provides an explanation as to why this phenomenon, although general, has been observed only rarely.

Polymer hydrogels are widely used for many applications, such as drug delivery, cell harvesting and culturing, tissue

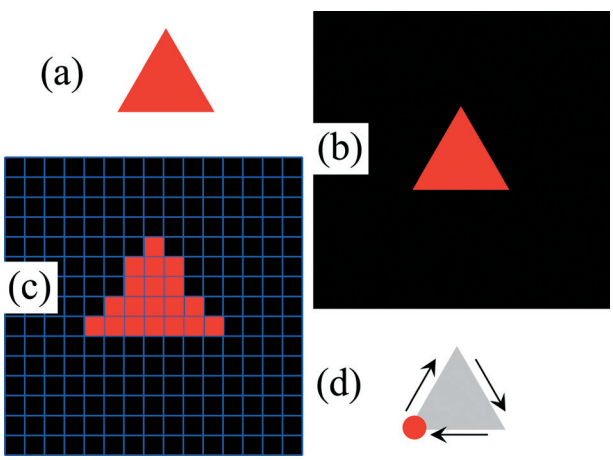

Fig. 1 Illustration of photopolymerization methods. (a) Desired triangular hydrogel. (b) Mask lithography. The opaque mask (black) has a triangular transparent window. The mask is placed directly on top of the sample containing the monomer solution and illuminated with uniform light (red). (c) Digital projection lithography. A computer projector display is imaged onto the monomer sample. The black squares are pixels not illuminated and the red squares are illuminated pixels. (d) Scanning lithography. A focused laser beam (red disk) is scanned across the solution containing the monomer to form the desired triangular gel.

[a] *School of Mechanical Engineering, Chonnam National University, South Korea*
[b] *Department of Physics, Brandeis University, USA. E-mail: fraden@brandeis.edu*
[c] *Department of Chemistry, Brandeis University, USA*

† Electronic supplementary information (ESI) available: Videos SI and SII showing photopolymerization *in situ*. See DOI: 10.1039/c4lc00158c

engineering and microfluidics.[1–10] Here, we focus on the hydrogel poly-*N*-isopropylacrylamide (pNIPAAM), a member of a subclass of hydrogels whose volume varies with both temperature and pH, properties that have frequently been exploited for applications, such as cell harvesting, surfaces for cell cultures[11–13] and for microactuators incorporated in microfluidic chips.[14–17]

In this paper we employed direct writing or maskless photopolymerization using a UV microscope system suitable for 2D and 3D printing, in which microstructured hydrogels are created by scanning a focused spot of UV light across the unpolymerized sample, as illustrated in Fig. 1(d). We constructed a UV microscope system for the photopolymerization of a NIPAAM gel using a combination of commercially available and homemade parts and demonstrated the possibility of fabricating pNIPAAM gel structures on the scale of tens of microns, which can be used as microactuators and tissue scaffolds.

We expected that photopolymerization of NIPAAM would result in gels whose shape mimicked that of illumination. Specifically, when the illumination profile was a uniform circular beam of light of 50 microns in diameter and the monomer solution was confined to a thin sample chamber of 10 microns in height, we expected to produce a gel of uniform density in the shape of a disk, as has been theoretically modeled and experimentally observed with hydrogels produced using stop–flow projection lithography.[5,18] We did indeed observe this behavior when using low light levels, or short time exposures, as shown in the first row of Fig. 2(A) and in Video SI.† Therefore, we were surprised to observe gels in the shape of a ring or annulus with a little gel in the center of the illuminated region at high illumination levels and long illumination exposures. We expected the gel to be densest in the brightest area; instead we observed the opposite, with the highest density gel found at the periphery of the illuminated region, a result published previously in a figure but not described in words or explained.[19] This phenomenon is illustrated in the bottom row of Fig. 2(A) and Video SII.† For thicker samples, on the order of 100 microns, we obtained partially hollow cylinders as shown in Fig. 2(B) and Video SII.† The shape of the gel resembles a water drinking glass as shown in Fig. 2(D). There is a solid gel on the end of the cylinder from which the light entered the sample, while the end of the cylinder from which the light exited the sample is open. Although it is not evident in Fig. 2, during the polymerization we observed a dim wave of a darker material rapidly growing out from the center of the illuminated region corresponding to a thin sheet of gel with a radius much larger than the illuminated region (Video SII†). The two observations, a concentrated ring of gel located at the edge of the disk of illumination and the extended thin sheet of gel, led us to conclude that reaction–diffusion considerations are governing the structure of the non-uniform gels. We note that this phenomenon is generic; we observed exactly the same non-uniform profile in another hydrogel, HEMA, shown in Fig. 2(C), which, in contrast to pNIPAAM, is non-thermosensitive.[20]

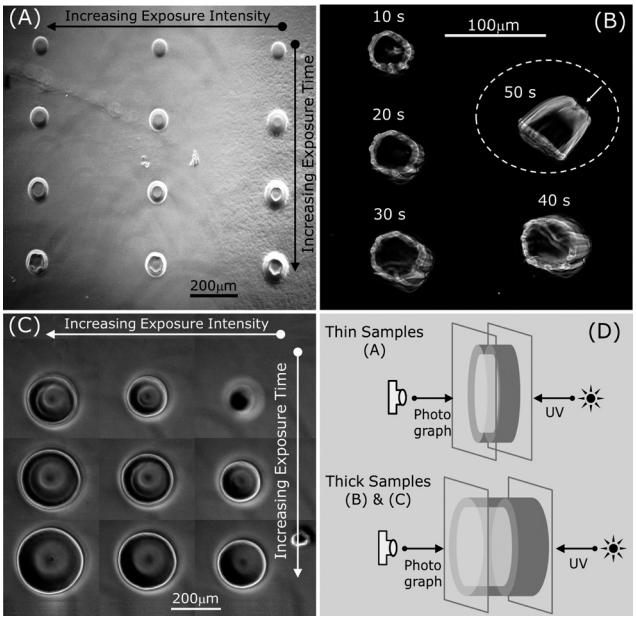

Fig. 2 pNIPAAM (A, B) and HEMA (C) gel patterning produced using a UV microscope. Movies of the temporal evolution of the polymerization are contained in the ESI.† The illumination profiles are uniform: 50 μm diameter in (A) and 100 μm diameter in (B) and (C). The UV light is incident perpendicular to the image plane and directed from the image towards the viewer. The images in Fig. 2A–C were photographed using a phase contrast microscope in the direction opposite to the UV illumination, as illustrated in Fig. 2D. (A) Variation of the exposure time and exposure intensity in a thin pNIPAAM sample (10 μm). See Video SI.† (B) Variation of the exposure time in a thick pNIPAAM sample (100 μm) with a moderate exposure intensity. The gel exposed for 50 seconds fell over after it was photopolymerized and in the photograph, it is lying on its side. The arrow points to the face upon which the UV light was incident. See Video SII.† (C) Variation of the exposure time and exposure intensity in a thick HEMA sample (100 μm), and (D) conceptual side-views of gels in thin and thick samples. Cross-sections perpendicular to the beam taken near the face on the UV incident side are solid disks, while cross-sections far from the UV incident side are annuli.

Furthermore, we also observed the phenomenon of ring formation using conventional lithography in which broad, unfocused light illuminated a mask in direct contact with the 100 μm thick chamber containing the monomer solution. Specifically, when we employed masks with holes of radii ranging from 100 μm to 500 μm in diameter, we observed the formation of rings of gels instead of what we expected, a uniform disk.

The utility of fabricating hydrogels using photopolymerization by either a mask-based or a projection-based method is facilitated when the shape of the resulting gel follows the illumination pattern. Therefore, the non-uniformity of the pNIPAAM gel illustrated in Fig. 2 will lead to the following drawbacks in applications: non-uniform polymerization concentrations in 3D printing of hydrogels, nonlinear response of pNIPAAM microactuators, nonlinear and uncontrollable drug release in drug delivery systems, and uneven cell culture and harvesting results in a pNIPAAM substrate. The objectives of this work are to elucidate the origin of the non-uniformity of the

pNIPAAM gel and to delineate the variables that are useful to control the polymerization procedure.

We expect that for most applications, conditions will be sought to avoid non-uniform gelation. However, there are circumstances where the production of gels in the shapes of rings or hollow cylinders instead of the intended disks or solid cylinders can be desirable. One example is the construction of hollow vesicles composed of pNIPAAM co-polymerized with a catalyst that exhibits self-oscillation and functions as a peristaltic pump.[21–23]

As a first step in the analysis of the non-uniformity of photopolymerized microscopic hydrogels, we developed a simplified reaction–diffusion kinetic model of the photopolymerization process. Next, we varied the key parameters controlling polymerization and through comparison of the experimental results with the theoretical ones we generated qualitative and quantitative understanding of the photopolymerization procedure of NIPAAM.

2. Direct patterning of NIPAAM using a LED microscope

2.1 Construction of the UV microscope

Polymerization was performed using a homemade ultraviolet (UV) microscope system that can be divided into three parts: UV illumination for photopolymerization, visible light imaging, and a motorized scanning stage. Fig. 3(A) is a photograph of the UV scanning microscope and Fig. 3(B) shows the schematic of its optical trains. Both the UV illumination and visible imaging optics are based on Köhler epi-illumination with an infinity corrected microscope objective lens.

The UV illumination consists of the following components arranged sequentially in a Köhler illumination geometry: a UV LED (Nichia NCSU034A, 385 nm, 350 mW), an aspheric condenser lens (Thorlabs A240TM-A, f_c = 8 mm, NA = 0.50), aperture and field diaphragms (Thorlabs SM1D12D), a transfer lens (f_t = 30 mm achromat), a beam-splitter cube (Thorlabs CM1-DCH) holding a dichroic beam-splitter with an edge wavelength of 416 nm (Semrock FF416-Di01-25 × 36) and an infinity corrected microscope objective lens (Nikon Plan Fluor 40×, N.A. = 0.75). When the field aperture was 300 μm in diameter, the focused beam spot on the sample surface was about 50 μm in diameter. The exposure intensity in the sample plane was measured and calibrated by an optical power and energy meter (Thorlabs, PM100D). The illumination is uniform, as demonstrated in Fig. 3(C) with a 100 μm spot size.

The function of the imaging arm is to visualize the polymerization of the pNIPAAM gel *in situ*. The illumination branch of the imaging arm is also set-up with Köhler illumination, with the components arranged sequentially. First, the light source is a red LED (Philips LumiLED, 630 nm, 350 mA), chosen so as not to affect the photoinitiator, followed by a condenser lens (f_c = 15 mm), angular and field apertures (Thorlabs SM1D12D), a transfer lens (f_t = 50 mm achromat), and a 50 : 50 beam-splitter (Thorlabs BSW10R). In addition,

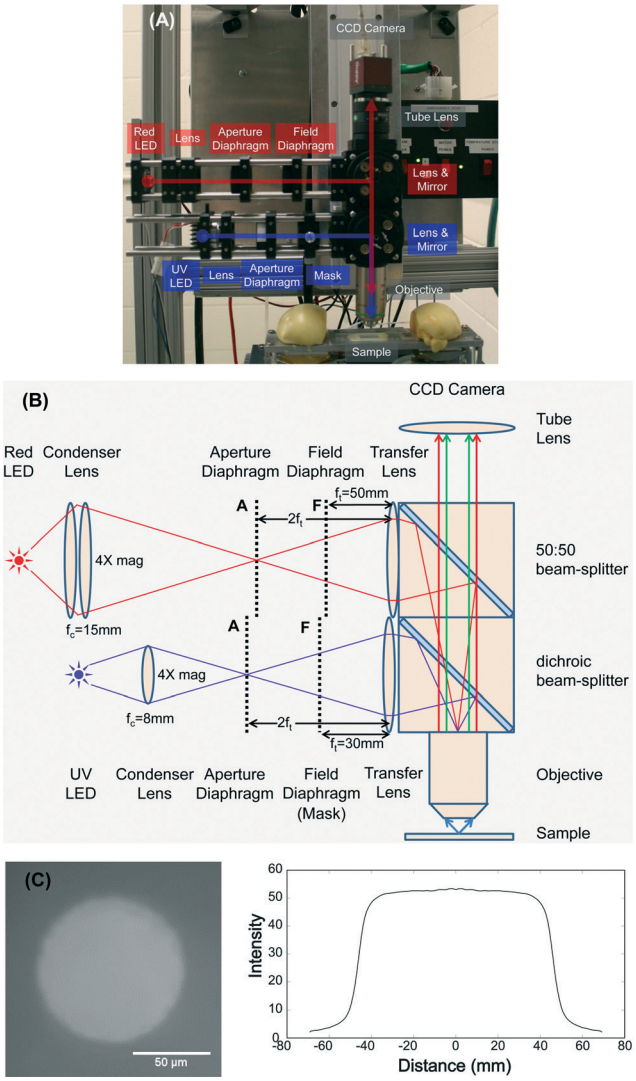

Fig. 3 Photopolymerization using UV illumination: (A) a UV fluorescence and visible light microscope and (B) a schematic of optical paths. (C) Photograph of UV illumination in the sample plane. Light of 385 nm wavelength is reflected from a polished silicon wafer. The adjacent profile shows the circularly averaged intensity taken from the photograph.

a digital USB CCD camera was installed in order to record images of the entire process of the NIPAAM polymerization.

The motorized *X*–*Y*–*Z* stage, which was not shown in Fig. 3, is based on stepping motor driven stages. The *X*–*Y* axis is used to scan the sample through the focused UV LED beam and the *Z* axis is used to translate the optics and thereby focus the UV LED beam at different heights in the NIPAAM sample.

2.2 Preparation of NIPAAM samples using a simple micro-channel chamber

To conduct photopolymerization experiments of a NIPAAM gel using our UV microscope system, we prepared a NIPAAM solution that consists of a NIPAAM monomer, a BIS cross-linker, Irgacure 819 dissolved in DI water, and methanol

(MeOH). The composition of our "nominal" NIPAAM solution, formulated without adding any of the terminator TEMPO (tetramethylpiperidinyloxy), is listed in Table 1.

Then we fabricated a simple microchannel chamber using a microscope slide, a cover glass, double sided tape with thickness of 10 μm, and paraffin wax. The preparation procedure of NIPAAM samples is shown in Fig. 3 and summarized as follows.

- Preparation of a clean microscope glass slide (25 × 75 × 1 mm).
- Attachment of two pieces of strip-shaped double sided tape to make parallel walls of a simple channel on the slide glass. The height of the microchannel is determined by the thickness of the double sided tape.
- Assembly of a cover glass (22 × 22 × 0.13–0.16 mm) on the double sided tape to make a chamber with a height of 10 μm composed of a simple channel.
- Injection of the NIPAAM solution into the simple channel. The capillary force in the microchannel easily draws the NIPAAM solution into the channel.
- Sealing of both ends of the microchannel with paraffin wax.

2.3. Measurement methods of a micro NIPAAM gel structure

To visualize the polymerization process *in situ*, shown in Videos SI and SII,† we used the visible light branch of our microscope, shown in Fig. 3. The sample geometry used in all of our experiments and videos is illustrated in Fig. 4. After polymerization, we removed the sample and imaged the gels using a phase contrast microscope (Nikon, Japan) and a laser confocal scanning microscope (Axio Observer, Zeiss, Germany). To render the pNIPAAM fluorescent for confocal microscopy, we added a small amount of a functionalized ruthenium probe (0.34 mM) in the NIPAAM solution before the photopolymerization of NIPAAM. The ruthenium probe, Ru(II)(bipy)$_2$(*N*-allyl-40-methyl-[2,20-bipy]-4-carboxamide),[24] is covalently attached as a pendant chain to the pNIPAAM backbone and has an excitation wavelength of 488 nm and an emission wavelength of 560 nm. After the photopolymerization, the non-polymerized NIPAAM solution and the unbound ruthenium probe are washed away. After flushing, the only ruthenium probe remaining is what was covalently attached to the polymerized NIPAAM structure. We assume that the density of the microscopic pNIPAAM gel is proportional to the density of the probe, which we further assume is proportional to the fluorescence intensity. We quantitatively measure the fluorescence using a laser confocal scanning microscope.

Table 1 Composition of the nominal NIPAAM solution

Contents	Function	Amount
NIPAAM (*N*-isopropylacrylamide)	Monomer	40.0 mg
NMBA (*N*,*N*′-methylenebisacrylamide)	Cross-linker	0.7–0.8 mg
Irgacure 819	Photoinitiator	0.5 mg
TEMPO	Terminator	0.0 mg
Methanol (MeOH)	Solvent	70.0 μl
DI water	Solvent	50.0 μl

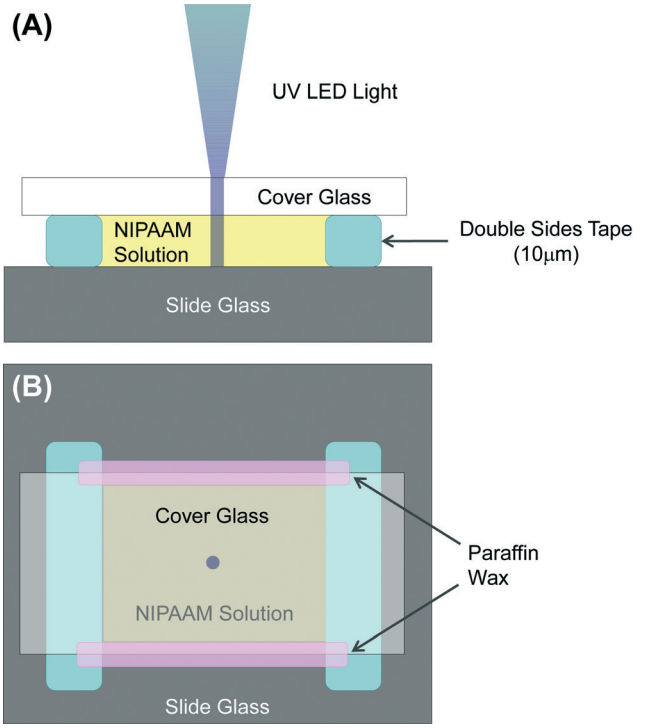

Fig. 4 NIPAAM sample preparation using a simple micro-channel chamber: (A) the side view and (B) the top view.

3. Simulation study using a simplified reaction–diffusion kinetic model

3.1 Simplified reaction–diffusion kinetic modeling

Building on previous kinetic models of free radical polymerization,[18,25–28] we developed a simplified reaction–diffusion kinetic model based on three processes, initiation, polymerization and termination, illustrated in Fig. 5. Initiation consists of two steps. In step (0), light converts the photoinitiator, PI, into an activated species, PI*. Light is absorbed in this process leading to an exponential decrease in the intensity with the sample depth, z. In step (1), the activated photoinitiator converts a monomer, m, into a free radical monomer, p^*.

The second process consists of free radical polymerization in which the radical, p^*, reacts with a monomer, forming a bond and transferring the free electron to the end of the growing polymer. This results in a distribution of chains of different lengths, each with one radical attached to the end, the kinetics of which can be described by a large set of rate equations. We lump the entire second process into one reaction, step (2): $p^* + m \rightarrow p^* + p$. In this approximation, we neglect the polymer length distribution and the fact that the polymer and the radical are attached. In this model, each time a radical and a monomer interact, a polymer is created. To represent the fact that polymers have a much higher molecular weight than monomers, we set the diffusion constant of a polymer to zero and for simplicity, assume all of the other species have equal diffusion constants. In our model, we consider chain propagation to be the principal process for polymer growth. To form a gel in the experiment, a small amount of cross-linker is added, which

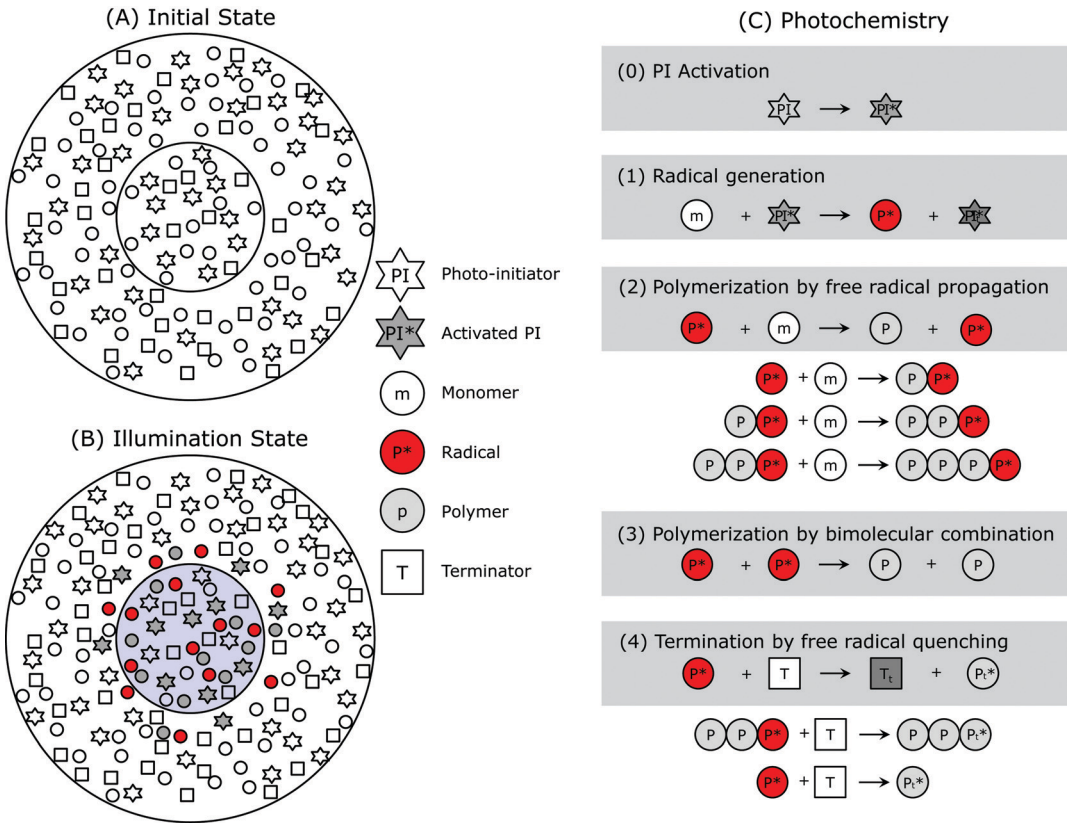

Fig. 5 Concept schematics of photochemistry in photopolymerization using an UV microscope: (A) the initial state, (B) illumination state, and (C) photochemistry (the non-shaded portions of steps (2) and (4) are expected to occur in actuality, but only the shaded schematic reactions are included in the model).

bonds two chains together. In this model, we neglect cross-linking entirely. Experimentally, we observe that stable gels form once the polymer concentration exceeds a critical threshold.

The third process consists of termination, which can occur in two different ways. First, if two radicals react, we consider the reaction to produce two polymers and consume the two radicals, shown in step (3). Second, if a radical reacts with a terminator, we consider the terminator and the radical to be consumed but no polymer is produced, shown in step (4). This is a subtle point. In reality, if the radical is attached to the end of a polymer, then when the radical is quenched, by either a terminator or another radical, a polymer is formed, as shown in step (4). However, if the radical hasn't been incorporated in a polymer and is still a monomer, albeit activated, then when it is quenched by a terminator, it would form an inert monomer and not a polymer. Since in our model, the radical and the polymer are treated as being independent, we assume that termination of a radical does not produce a polymer.

We explored several variants of this model, some simpler and some more complex. For example, we made one model in which we assumed that light directly activated the monomers and thereby we eliminated the photoinitiator and the additional terminator, leading to a model with only 3 components: monomer, radical and polymer. This minimal model produced results evocative of the experiment and helped us develop a clear conceptual understanding of the principal phenomenon. While inclusion of the photoinitiator and terminator leads to more complicated equations, the scheme presented in Fig. 5 strikes a balance between retaining the essential features of the experimental system and remaining simple enough to be understood conceptually.

A schematic of the kinetics of the processes included in our model is illustrated in Fig. 5 and the resulting kinetic equations are

$$\frac{\partial PI}{\partial t} = -k_{\mathrm{i}}\mathrm{PI}_0 \exp(-\alpha z) + D_{\mathrm{PI}}\nabla^2\mathrm{PI} \tag{1}$$

$$\frac{\partial PI^*}{\partial t} = k_{\mathrm{i}}\mathrm{PI}\exp(-\alpha z) - k_{\mathrm{r}}\mathrm{PI}^* m + D_{\mathrm{PI}^*}\nabla^2\mathrm{PI}^* \tag{2}$$

$$\frac{\partial m}{\partial t} = -k_{\mathrm{r}}\mathrm{PI}^* m - k_{\mathrm{p}} p^* m + D_{\mathrm{m}}\nabla^2 m \tag{3}$$

$$\frac{\partial p^*}{\partial t} = k_{\mathrm{r}}\mathrm{PI}^* m - k_{\mathrm{s}} p^* p^* - k_{\mathrm{t}} p^* T + D_{p^*}\nabla^2 p^* \tag{4}$$

$$\frac{\partial p}{\partial t} = k_{\mathrm{p}} p^* m + k_{\mathrm{s}} p^* p^* \tag{5}$$

$$\frac{\partial T}{\partial \mathrm{t}} = -k_{\mathrm{t}} p^* T + D_{\mathrm{T}}\nabla^2 T \tag{6}$$

where PI, PI*, m, p^*, p, and T denote the concentrations of the photoinitiator, activated photoinitiator, monomer, free radical monomer, polymer, and terminator, respectively. k_i, k_r, k_p, k_s, and k_t are the rate constants of activated photoinitiator generation, free radical generation, chain propagation, bimolecular chain termination, and chain termination by the terminator, respectively. In addition, D_{PI}, D_{PI^*}, D_m, D_{p^*}, and D_T are the diffusivity coefficients of the photoinitiator, activated photoinitiator, monomer, free radical, and terminator, respectively. The polymer was assumed to be immobile because the polymer has a high molecular weight and will cross-link into a gel; therefore the polymer diffusion constant was set to zero. The rate of photoinitiator radical production, $k_i\mathrm{PI}\exp(-\alpha z)$, in eqn (1) and (2) can be expressed in terms of the UV intensity as[15]

$$k_i\mathrm{PI}\exp(-\alpha z) = \varphi\varepsilon I_0\mathrm{PI}\exp(-\varepsilon\mathrm{PI}z) \tag{7}$$

where φ is the quantum efficiency, ε is the extinction coefficient, I_0 is the incident light intensity, and z is the depth of the NIPAAM solution.

For simplicity, we assumed that all diffusivity coefficients (D_{PI}, D_{PI^*}, D_m, D_{p^*}, and D_T) are equal to D. Next, we non-dimensionalized the reaction–diffusion kinetic model with 7 dimensionless constants, assuming axisymmetry, in cylindrical coordinates.

$$\frac{\partial \mathrm{PI}_n}{\partial \tau} = -K_I\mathrm{PI}_n\exp\left(-\phi_s\mathrm{PI}_n\xi\right) + \frac{1}{r_n}\frac{\partial \mathrm{PI}_n}{\partial r_n} + \frac{\partial^2 \mathrm{PI}_n}{\partial r_n^2} + K_Z\frac{\partial^2 \mathrm{PI}_n}{\partial \xi^2} \tag{8}$$

$$\frac{\partial \mathrm{PI}_n^*}{\partial \tau} = K_I\mathrm{PI}_n\exp\left(-\phi_s\mathrm{PI}_n\xi\right) - K_R\mathrm{PI}_n^*M + \frac{1}{r_n}\frac{\partial \mathrm{PI}_n^*}{\partial r_n} + \frac{\partial^2 \mathrm{PI}_n^*}{\partial r_n^2} + K_Z\frac{\partial^2 \mathrm{PI}_n^*}{\partial \xi^2} \tag{9}$$

$$\frac{\partial M}{\partial \tau} = -K_R\mathrm{PI}_n^*M - K_pP^*M + \frac{1}{r_n}\frac{\partial M}{\partial r_n} + \frac{\partial^2 M}{\partial r_n^2} + K_Z\frac{\partial^2 M}{\partial \xi^2} \tag{10}$$

$$\frac{\partial P^*}{\partial \tau} = K_R\mathrm{PI}_n^*M - K_SP^*\ P^* - K_TP^*\ T_n + \frac{1}{r_n}\frac{\partial P^*}{\partial r_n} + \frac{\partial^2 P^*}{\partial r_n^2} + K_Z\frac{\partial^2 P^*}{\partial \xi^2} \tag{11}$$

$$\frac{\partial P}{\partial \tau} = K_PP^*M + K_SP^*P^* \tag{12}$$

$$\frac{\partial T_n}{\partial \tau} = -K_TP^*T_n + \frac{1}{r_n}\frac{\partial T_n}{\partial r_n} + \frac{\partial^2 T_n}{\partial r_n^2} + K_Z\frac{\partial^2 T_n}{\partial \xi^2} \tag{13}$$

where PI_n, PI_n^*, M, P^*, P, and T_n denote the non-dimensional variables (concentrations of the photoinitiator, activated photoinitiator, monomer, free radical, polymer, and terminator), which are defined as $\mathrm{PI} = \mathrm{PI}_n m_0$, $\mathrm{PI}^* = \mathrm{PI}_n^* m_0$, $m = Mm_0$, $p^* = P^*m_0$, $p = Pm_0$, and $T = T_n m_0$, where m_0 is the initial monomer concentration. r_n, ξ and τ denote the non-dimensional radius, depth and time and are defined as $r = r_n R, z = \xi H$, and $t = \tau\frac{R^2}{D}$, where R is the radius of the focused uniform UV beam, H is the height of the sample chamber, and $\frac{R^2}{D}$ is the time to diffuse the size of the illuminated region. The non-dimensional concentration variables are functions of space and time, r_n, ξ and τ, such that $\mathrm{PI}_n(r_n, \xi, \tau)$, $\mathrm{PI}_n^*(r_n, \xi, \tau)$, $M(r_n, \xi, \tau)$, $P^*(r_n, \xi, \tau)$, $P(r_n, \xi, \tau)$, and $T_n(r_n, \xi, \tau)$. Finally, the simplified reaction–diffusion kinetic model (eqn (8)–(13)) has 7 dimensionless constants (K_I, K_R, K_P, K_S, K_T, K_Z, and ϕ_ε), which are defined as

$$\begin{aligned} &K_I = \frac{R^2}{D}\varphi\varepsilon I_0,\ K_R = \frac{R^2}{D}m_0k_r,\ K_P = \frac{R^2}{D}m_0k_p,\ K_T = \frac{R^2}{D}m_0k_t,\\ &K_S = \frac{R^2}{D}m_0k_s,\ K_Z = \frac{R^2}{H^2},\ \varphi_\varepsilon = \varepsilon m_0H \end{aligned} \tag{14}$$

Roughly, K_I and K_R govern initiation, K_P governs polymerization, K_T and K_S govern termination, and K_Z and ϕ_ε control whether the polymerization has a two or three dimensional character. The dimensionless constants, K_R, K_P, K_T and K_S, are the ratios of reaction rates to diffusive rates and are known as Damköhler numbers.

3.2 Simulation method

We utilize an axisymmetric simulation volume for the non-dimensional kinetic models of eqn (8)–(13) in the shape of a cylinder of dimensionless radius $r_n = 20$ and height $\xi = 1$ in order to represent a sample confined between two pieces of glass, located at $\xi = 0$ and $\xi = 1$. We run the simulation for a total dimensionless time of $\tau = 20$. The UV beam, with the incident perpendicular to the two pieces of glass, uniformly illuminates only the central region of $0 \le r_n \le 1$, during a non-dimensional exposure time, most often for a duration of $\Delta\tau = 2$.

To proceed, first we use the following initial conditions: $\mathrm{PI}_n(r_n, \xi, \tau = 0) = 1$, $\mathrm{PI}_n^*(r_n, \xi, \tau = 0) = 0$, $M(r_n, \xi, \tau = 0) = 1$, $P^*(r_n, \xi, \tau = 0) = 0$, $P(r_n, \xi, \tau = 0) = 0$, and $T_n(r_n, \xi, \tau = 0) = T_0$ for the entire sample volume, $0 \le r_n \le 20$ and $0 \le \xi \le 1$. Second, we employ mixed boundary conditions. We use constant concentration boundary conditions along the surface of the cylindrical portion of the volume and no-flux boundaries along the end caps of the cylinder, corresponding to the glass slides containing the sample. However, we use a large enough volume and short enough time that the same results are obtained when using constant concentration and no-flux boundary conditions on the cylindrical surface. Physically this means that the sample container is large enough so that chemicals at the boundary don't have time to diffuse to the illuminated region during the experiment. The constant chemical boundary conditions along the cylindrical wall are $\mathrm{PI}_n(20, \xi, \tau) = 1$, $\mathrm{PI}_n^*(20, \xi, \tau) = 0$, $M(20, \xi, \tau) = 1$, $P^*(20, \xi, \tau = 0) = 0$, $P(20, \xi, \tau) = 0$, and $T_n(20, \xi, \tau) = T_0$. The remaining boundaries that form the end cap of the cylinder have no-flux

conditions for all chemical variables (*e.g.*, $\nabla M(r_n, 0, \tau) = 0$, and $\nabla M(r_n, 1, \tau) = 0$).

In general, boundary conditions matter; the boundary conditions we have chosen are appropriate for cases where there is a large container holding the monomer but only a small part of the container is exposed to light. In contrast, if the entire container is illuminated with light, then there would be no-flux boundaries imposed at the edge of the illumination region, and we speculate that for this case, the gel will always be uniform.

3.3 Simulation results I: effect of concentration and intensity on photopolymerization

We numerically solved the simplified reaction–diffusion kinetic model simulation using a finite-element solver, COMSOL 3.5a (COMSOL, Inc.). In our numerical studies of photopolymerization, we varied the parameters, such as exposure time, exposure intensity, monomer concentration, and terminator concentration because these parameters can be easily changed in experiments.

There are 7 dimensionless variables listed in eqn (14) and to reduce the parameter space we imposed some restrictions. The dimensionless constants K_R, K_P, K_T, and K_S, have the same functional form and are proportional to the initial monomer concentration, m_0; for simplicity we set them all equal to the same constant, K, which we call the "reaction" parameter. K, the ratio of the reaction rate to the diffusion rate, is the Damköhler number.

$K_Z = R^2/H^2$ is determined by the height of the chamber (H) and the focused UV beam radius (R); we set K_Z as a constant, 6.25, which was calculated from our sample cell's dimensions. K_I is proportional to the exposure intensity (I_0). Additionally, both the exposure time, $\Delta\tau$, and the initial terminator concentration (T_{n0}) can be readily changed in the simulation and experiment. After some exploration of the numerical model, we set conditions for the simulation, which we refer to as the "nominal" case with: $\Delta\tau = 2$, $K_I = 5$, $K = 10$, $\varphi_\varepsilon = 1$ and $T_{n0} = 0$. The nominal case corresponds to the zero added terminator, $T = 0$; therefore free radical propagation leads to polymerization outside the zone of illumination. The duration of exposure, $\Delta\tau = 2$, means that there is just sufficient time for molecules to diffuse across the zone of illumination. The rate constants, K, being of order 10 mean that reaction dominates over diffusion. Beginning with this nominal case, we sequentially varied one of the following four parameters: exposure time, exposure intensity, monomer concentration (and hence both the reaction parameter K and the light absorption parameter ϕ_ε), and initial terminator concentration, as indicated in Table 2.

Table 2 Parameters for simulated photopolymerization in Fig. 6[a]

Cases	Exposure time ($\Delta\tau$)	K_I	K	ϕ_ε	T_{n0}
Nominal case	2	5	10	1	0
Exposure time variation	0.2, 0.6, **2**, 6, 20	5	10	1	0
Exposure intensity variation	2	0.5, 1.5, **5**, 15, 50	10	1	0
Monomer concentration variation	2	5	1, 3, **10**, 30, 100	0.1, 0.3, **1**, 3, 10	0
Terminator concentration variation	2	5	10	1	**0**, 0.3, 1, 3, 10

[a] The entries in the 2nd to 5th rows list the simulation conditions that correspond to Fig. 6, rows A–D. The entries in grey boxes are the only parameters that vary, while the entries in the white boxes are held constant. Each grey box has five entries, corresponding to the five columns in Fig. 6. The first row has the conditions for the "nominal case" that appears once in each row in Fig. 6. In Fig. 6 the nominal case is highlighted by a bolded box. In Table 3, the nominal case conditions are indicated by a bold number.

Simulation results for the photopolymerization conditions in Table 2 are shown in Fig. 6, which shows cross-sectional views of selected portions of the polymer concentration. The cross-section that is displayed in both Fig. 6 and 7 was taken at the mid-plane of the simulation volume, ξ = 0.5. The identical nominal case appears once in each row of Fig. 6(A-3), (B-3), (C-3) and (D-1), denoted by a bold line enclosing the plot. The polymer concentration of the nominal case has the shape of a mountain with a flat top. The width of the polymer is much greater than that of the illuminated region. This is due to the diffusion of the radical monomer and the radical initiator outside of the illuminated region and the reaction with monomers to form polymers. First, when the exposure times were increased, illustrated in row A, the polymer concentrations increased and the polymer profile resembled a volcano with a crater forming at the top (A-4, A-5). Conversely, when the exposure times were decreased, the polymer concentrations also decreased overall and the polymer concentration showed a continuous convex mountain shape (A-1, A-2). Second, in row B, when the exposure intensities were varied, the simulation results were extremely similar to those of the exposure time variation. With higher exposure intensities, the polymer concentration profile resembles a volcano with a crater (B-4, B-5) and with lower exposure intensities, the polymer concentrations show a convex mountain shape (B-1, B-2). Third, we changed the initial monomer concentration and with it the reaction parameter K and the attenuation constant, ϕ_ε, which as seen in eqn (14) vary linearly with the monomer concentration. When we used higher monomer concentrations, the polymer concentration profile developed well defined volcano-like craters (C-4, C-5) and when we used lower monomer concentrations, the polymer concentrations were much decreased and resembled a simple convex mountain (C-1, C-2). Finally, when we added a terminator, the overall polymer concentrations were greatly decreased. With moderate amounts of the terminator, the polymer concentration profile became a cylinder, similar to the illumination profile (D-2, D-3). These are the optimal conditions for direct writing photopolymerization used in 3D printing. The terminator quenches any radicals that diffuse outside the illuminated region. When we increased the terminator concentration further, the polymer concentration was drastically decreased and the polymer profile again resembled a volcano with a crater (D-4, D-5).

The general trend, as shown in these simulation results (Fig. 6), is that the polymer concentration profile has a simple convex mountain shape in the limit of short exposure time, low exposure intensity, low monomer concentration and low terminator concentration, shown in the upper left portion of Fig. 6. However, at long exposure time, high exposure intensity, high monomer concentration and high terminator concentration, the polymer concentration profile resembles a volcano with a crater, shown in the lower right side of Fig. 6.

3.4 Simulation results II: temporal evolution of photopolymerization

The non-dimensional parameters of eqn (14), K_I, K_R, K_P, K_T, and K_S, are proportional to the ratio of the reaction rate, of

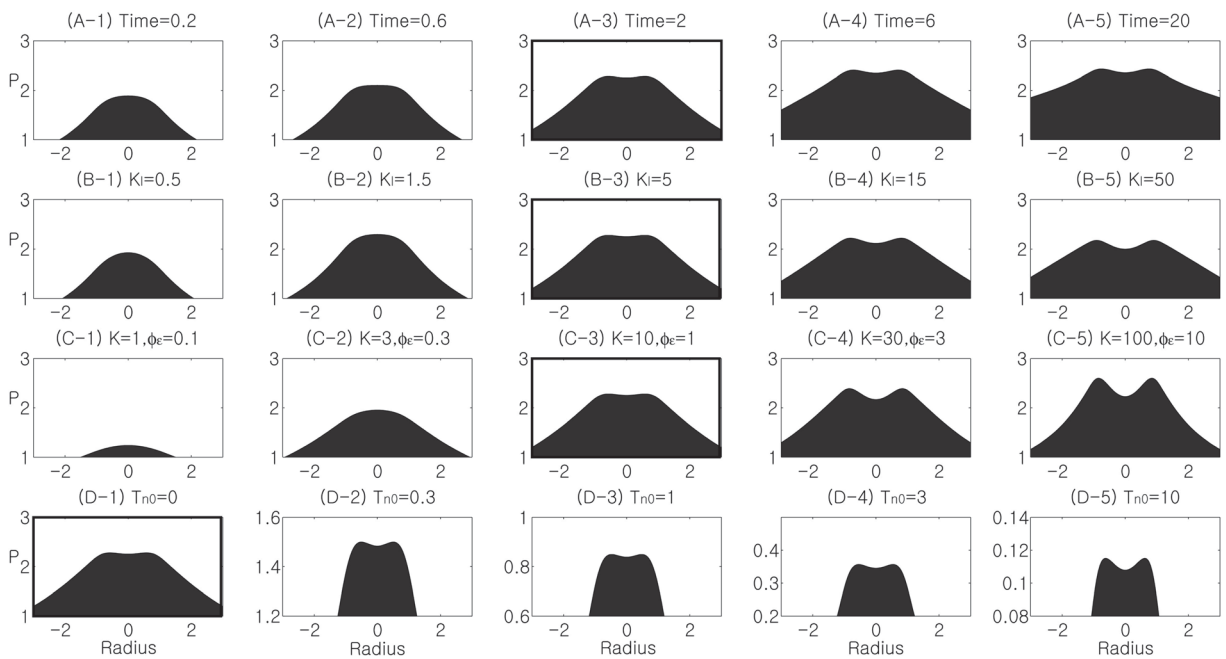

Fig. 6 Simulation results of the cross-sectional view, taken at height ξ = 0.5, of the polymer concentration as a function of the non-dimensional parameters. See Table 2 for the simulation values. The nominal conditions are used in the four cases (A-3, B-3, C-3, and D1) placed in a bolded box; $\Delta\tau$ = 2, r = 1, K_I = 5, K = 10, ϕ_ε = 1, T_{n0} = 0. In each row the nominal conditions are used and only the labeled quantities are varied. The values are listed in Table 2. A: exposure time ($\Delta\tau$), B: exposure intensity, C: reaction parameter (K) and absorption length (ϕ), and D: terminator concentration.

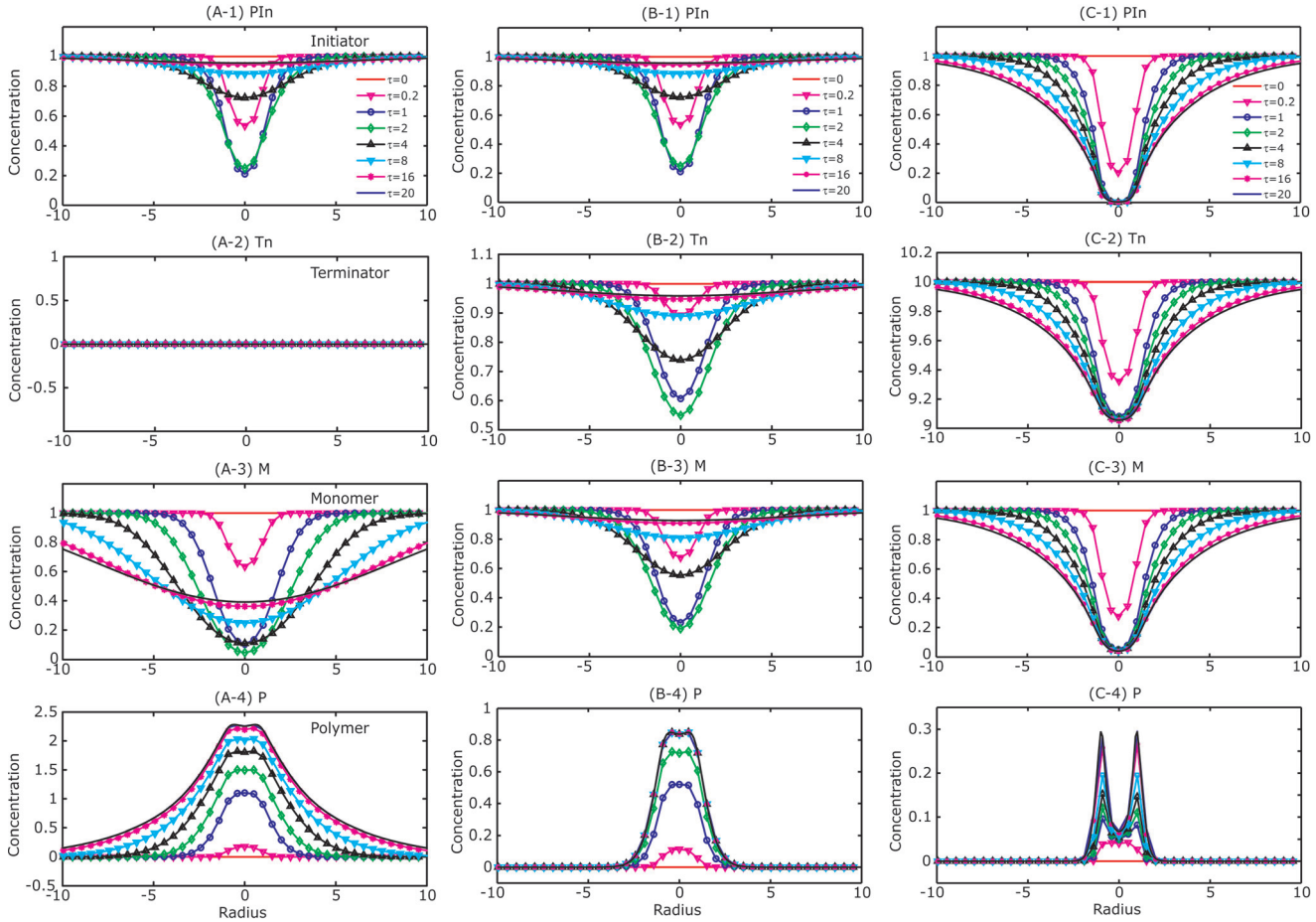

Fig. 7 Simulation results. Rows 1–4 show the temporal evolution of the (row 1) photoinitiator, (row 2) terminator, (row 3) monomer, and (row 4) polymer. In all cases, a uniform beam of light of radius $r = 1$ illuminates the sample. Cross-sections are taken at height $\xi = 0.5$. See Table 3 for the simulation values. A1–A4: diffusion dominated without a terminator (nominal case). Illumination duration: $\Delta\tau = 2$. The polymer concentration is uniform within the illuminated region, but extends far outside the zone of illumination. B1–B4: diffusion dominated with a terminator. Illumination duration: $\Delta\tau = 2$. In contrast to Fig. 7A4, the polymer concentration is largely confined to the illumination zone. C1–C4: reaction dominated. Illumination duration: $\Delta\tau = 20$. The polymer forms a hollow cylinder.

which k_p is one example, to the rate of diffusion across the illuminated region, D/R^2. Therefore, the photopolymerization process is diffusion dominated when we use small non-dimensional parameters. On the contrary, the process is reaction dominated when we use large non-dimensional parameters. Therefore, we considered two cases representing the limits of either reaction or diffusion domination. Table 3 lists three sets of conditions, one corresponding to the reaction dominant condition, and two to the diffusion dominant condition, with or without a terminator. The reaction dominant condition has a high exposure intensity, high monomer concentration and high terminator concentration. In contrast, the diffusion dominant condition has a low exposure intensity, low monomer concentration and low terminator concentration compared with the reaction dominant condition.

First, Fig. 7A1–A4 show the temporal evolution of four dimensionless concentrations: photoinitiator, terminator, monomer and polymer at the nominal condition. During the exposure time of duration $\Delta\tau = 2$, the photoinitiator and the monomer concentrations are decreased in the exposed region ($r_n \leq 1$) to almost zero. After the exposure time, the photoinitiator and the monomer concentrations slowly recover to near the initial concentrations through the diffusive influx of the photoinitiator and the monomer from outside of the illuminated region. As there is no terminator, the polymer extends far outside the illuminated region and the final polymer profile resembles a flat topped mountain.

Second, Fig. 7B1–B4 show the temporal evolution of the concentrations for the diffusion dominated condition of short

Table 3 Parameters for simulated photopolymerization in Fig. 7[a]

Cases	Exposure time	K_I	K	ϕ_ε	T_{n0}
Diffusion dominated w/o a terminator	2	5	10	1	0
Diffusion dominated w/ a terminator	2	5	10	1	1
Reaction dominated	20	50	100	10	10

[a] The first row corresponds to Fig. 7A, the second row to Fig. 7B, and the third row to Fig. 7C.

exposure, weak intensity, and low concentration, with a moderate amount of terminator. As in Fig. 7A1–A4, the monomer has ample time to diffuse across the illuminated region before any reaction occurs and consequently the polymer concentration slowly increases over time, developing into a simple convex mountain shaped profile. In contrast to Fig. 7A1–A4, a little polymer appears outside the illuminated region due to the presence of the terminator, resulting in a gel whose concentration profile mirrors the illumination profile.

Third, Fig. 7C1–C4 show the temporal evolution of the four dimensionless concentrations: photoinitiator, terminator, monomer and polymer, for the reaction dominated conditions of long exposure time, $\Delta\tau$ = 20, high exposure intensity, and high terminator concentration. Due to the high intensity, the photoinitiator and the monomer concentrations quickly decrease to zero in the illuminated region, $r_n \leq 1$. The terminator concentration in Fig. 7C-2 remains high throughout the simulation volume, which causes the polymer concentration to be very low outside of the illuminated region. The polymer grows over time due to the influx of monomers outside the illuminated region. Because both the monomer and the photoinitiator are depleted inside the illuminated region, the polymer can only grow at the edge of the illuminated region. This explains the hollow, cylindrical shape of the polymer in the reaction dominated regime.

It is noteworthy that for all three conditions the polymer concentration profile is convex for short times as illustrated for $\Delta\tau$ = 0.2 in Fig. 7. This is because for short exposure times there is insufficient time for the monomer to diffuse into the illuminated zone to replenish the material that is polymerized. The lesson is that short exposure times ($\Delta\tau \ll 1$) produce uniform gels regardless of whether the system is reaction or diffusion dominated.

4. Experimental results and discussions

4.1 Parametric study in photopolymerization of NIPAAM gels

In this section, we experimentally tested the effects of controllable parameters, such as exposure time, exposure intensity, monomer concentration, and terminator concentration on the photopolymerization of pNIPAAM gels. The measured images of the final, polymerized NIPAAM structures are displayed in Fig. 8. Confocal microscope images are shown, along with

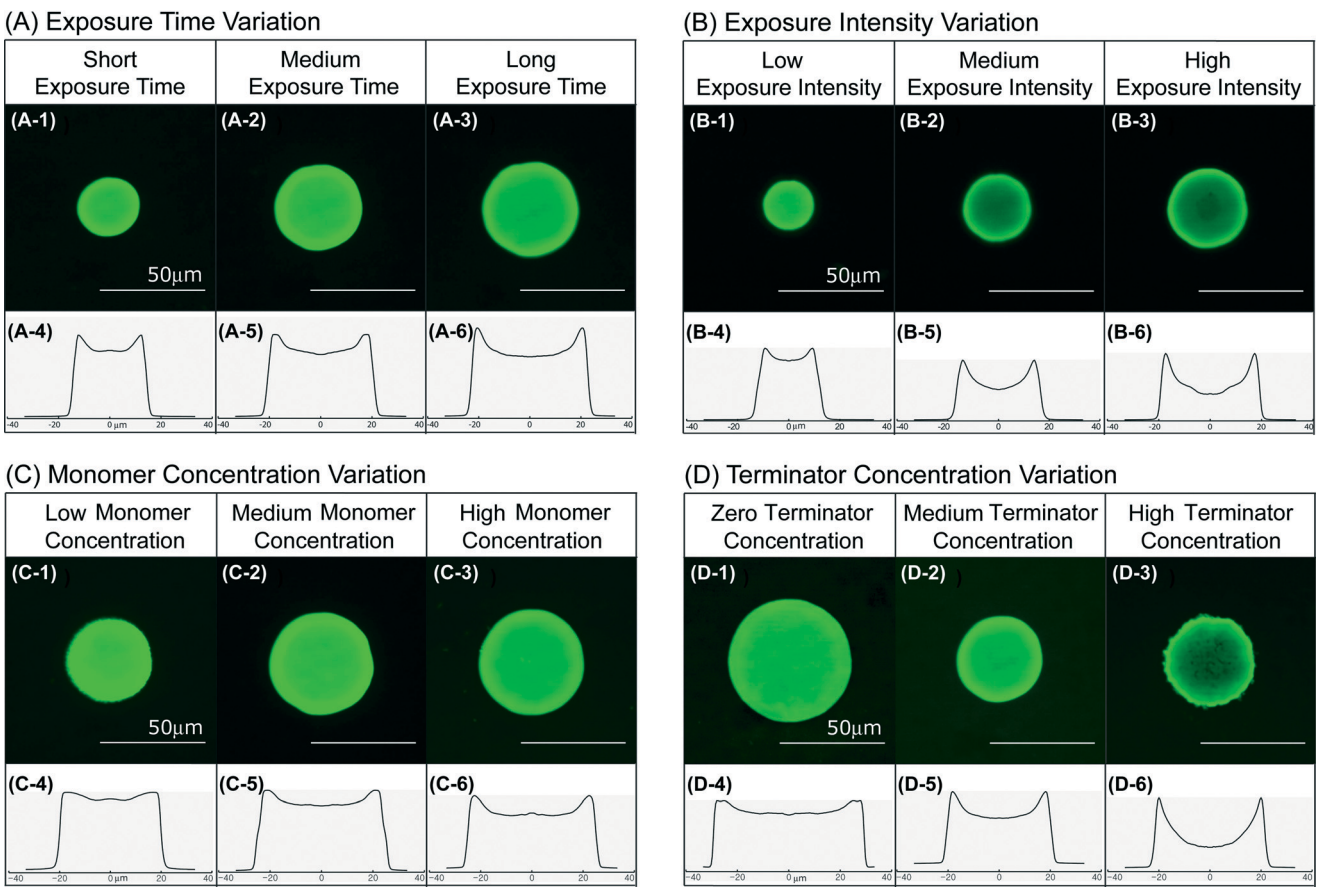

Fig. 8 Experimental results. The concentration profile of photopolymerized pNIPAAM gels. Confocal microscope images are focused in the mid-plane of a 10 μm thick sample. The adjacent line plots are circular averages of the confocal images. The diameter of the illumination beam is 50 μm. Phase contrast images of gels are shown in Fig. 2, and videos of the polymerization process recorded using an epi-illumination bright field microscope are shown in Videos SI and SII.† Variation of (A) the exposure time, (B) exposure intensity, (C) monomer concentration, and (D) terminator concentration.

circularly averaged intensity profiles of the confocal microscope images. Our experiments were guided by the results of the previous section, in which we simulated photopolymerization using a reaction–diffusion model.

We observed the sample *in situ* during UV illumination using our microscope. Movies of the polymerization process are shown in the ESI.† For very low doses of light, we observed the growth of weak optical contrast in the UV exposed region, implying that polymerization was taking place. However, after we ceased illumination the contrast gradually disappeared. We interpreted this to imply that the polymer concentration was subcritical and that a gel did not form so that after some time diffusion acted to homogenize the sample. In what follows, the conditions are such that the polymerized structures are permanent gels. In terms of our model, we assume that gelation occurs once the polymer concentration exceeds a critical value. As that value is observed to be small, we neglect it in our model.

a. Variation of exposure time. We performed direct patterning of NIPAAM gels as a function of exposure time, shown in Fig. 8A. In this test, the intensity of the 50 μm diameter UV beam measured in the sample plane was 1.1×10^3 W m^{-2} and the exposure time was varied: 10, 15, and 20 seconds. The composition of the NIPAAM solution, formulated without a terminator and referred to as the "nominal" condition, is listed in Table 1. At the shortest exposure time (10 s), the diameter of the poly-NIPAAM is smaller than the exposed UV beam size (50 μm). However, as the exposure times increase, the diameters of the poly-NIPAAM gels increase. In addition, for all exposure times, the poly-NIPAAM gels show clear ring-type patterns in which the gel is denser at the perimeter. The non-uniformity is accentuated with increasing exposure time. Therefore, to obtain a uniform structure of the poly-NIPAAM gel on the scale of tens of microns, it is necessary to select a short exposure time of the focused UV beam.

b. Variation of exposure intensity. Fig. 8B shows the effect of exposure intensity on the photopolymerization of NIPAAM. We varied the intensity of a 50 μm diameter UV beam for the following values: 1.1×10^3, 2.2×10^3, and 4.4×10^3 W m^{-2} at a constant exposure time of 10 seconds, using the nominal composition of NIPAAM solution, listed in Table 1. As the exposure intensity increases, the diameter of the pNIPAAM gel increases, but, to a greater extent, the non-uniformity of the gel increases, with the gel concentration being low in the center of the illuminated region, then increasing to the edge of the gel, before abruptly decreasing to zero. Increasing the light intensity has a similar effect on the gel structure as increasing the exposure time. At low intensity, the system is diffusion limited and as the intensity is increased, the system becomes increasingly reaction dominated. Consequently, a low value of the exposure intensity of the focused UV beam is required to produce a uniform pNIPAAM gel on the scale of tens of microns.

c. Variation of monomer concentration. Fig. 8C shows the effect of NIPAAM monomer concentration on the photopolymerization of NIPAAM. Starting with the nominal NIPAAM solution in Table 1, in which the monomer concentration was 333 mg ml^{-1}, one lower monomer concentration of 167 mg ml^{-1} and one higher value of 500 mg ml^{-1} were investigated. In addition, we adopt the nominal exposure intensity of 2.2×10^3 W m^{-2} and the exposure time of 15 seconds. At the low monomer concentration, the diameter of the poly-NIPAAM microstructure is about 40 μm, which is 10 μm less than the diameter of the illuminated region. The concentration profile of the polymer is nearly uniform. As the monomer concentration is increased, the diameter of the gel matches the diameter of the illuminated region and the concentration profile becomes increasingly non-uniform. At low monomer concentration, the system is diffusion limited and as the concentration is increased, the system becomes increasingly reaction dominated. Therefore, the monomer concentration is also an important parameter for controlling the uniformity of a pNIPAAM gel on the micron scale.

d. Variation of terminator concentration. Fig. 8D shows the effect of the terminator concentration on the photopolymerization of NIPAAM. Starting with the nominal NIPAAM solution in Table 1, in which the monomer concentration was 333 mg ml^{-1}, we added the radical terminator, TEMPO (tetramethylpiperidinyloxy) of 0.05 and 0.1 mg. In addition, we used the nominal exposure intensity, 2.2×10^3 W m^{-2}, and the exposure time, 10 s. As the terminator concentration increases, the diameters of the pNIPAAM microstructures decrease. More dramatically, the concentration profile becomes extremely non-uniform as the terminator concentration is increased, with a hollow interior and a very sharp exterior edge. The terminator inhibits chain propagation of the free radical in the photopolymerization, thereby preventing any gel from forming outside of the illuminated region. Polymerization is suppressed inside the illuminated region because initially all of the monomers are consumed by being converted into radicals and then either terminated or polymerized. Once all of the monomers in the interior of the illuminated region are consumed, the new monomer can only arrive from outside the illuminated region. Since the intensity is high, the newly arrived monomer at the periphery of the illuminated region is either converted into a radical and grows into a polymer or is terminated. Neither the unexcited monomer nor the radical that arrive at the periphery survive long enough to diffuse to the center of the illuminated region. Therefore, high terminator concentration leads to a hollow interior, but low terminator concentration leads to extended, diffuse boundaries of the gel extending beyond the illuminated region.

4.2 Discussion

a Summary. In this paper, we used a UV microscope system to photopolymerize NIPAAM hydrogels of diameter 50 microns. Surprisingly, we discovered conditions in which illumination with a beam of light of a uniform, circular cross-section produced a hollow cylinder of gel, instead of

the expected solid cylinder of gel. To understand the origin of this phenomenon, we developed a simplified reaction–diffusion model of the gelation process and compared theory with experiment. In this study, we experimentally varied the exposure time, exposure intensity, monomer concentration, and terminator concentration. First, when we used long exposure time or high exposure intensity, the resulting pNIPAAM gel was non-uniform. Second, high monomer concentration also affects the uniformity of the pNIPAAM gel. At low monomer concentration, the diameter of the microstructure decreases drastically and at high concentration, the gel becomes non-uniform. Finally, the terminator concentration also influences the uniformity of pNIPAAM. As the terminator concentration increases, the diameter of the microstructure decreases. At high terminator concentration, pNIPAAM gels form as hollow cylinders with very sharp edges.

b Interpretation. Our model of photopolymerization of hydrogels is appropriate for the case where polymerization is induced in a small volume of a much larger sample. We found that the photopolymerization process of a NIPAAM gel can be categorized into four regimes controlled by two independent dimensionless numbers. The first number is dimensionless time, $\tau = tD/R^2$, where $\tau = 1$ corresponds to the time needed for a monomer to diffuse across the illuminated region. The second is the Damköhler number, $K = mkR^2/D$, the ratio of the reaction rate to the diffusion rate. In photopolymerization there are Damköhler numbers for each diffusing and reacting chemical component. In our theoretical model we consider 4 distinct Damköhler numbers, but to simplify the process in order to develop physical intuition we considered that all 4 Damköhler numbers were equal. The polymerization is reaction dominated for $K \gg 1$ and diffusion dominated for $K \ll 1$. Gels are always uniform for $\tau \ll 1$ or $K \ll 1$ and non-uniform only when both $\tau > 1$ and $K > 1$. The reaction dominant regime occurs under conditions of high exposure intensity, high monomer concentration and high terminator concentration. In this regime, the monomer inside the uniformly illuminated zone is rapidly consumed. The new monomer diffuses in from outside the illuminated region and polymerizes as soon as it contacts the outer boundary of the beam of light, leading to the production of a hollow cylinder. In contrast, the diffusion dominant regime occurs for low exposure intensity, low monomer concentration and moderate terminator concentration. The monomer reacts infrequently and has more than enough time to diffuse across the illumination zone before interacting with a radical or a terminator, leading to the production of a gel whose concentration profile resembles the illumination profile. Consequently, to produce pNIPAAM gels whose concentration profile resembles the illumination profile, one should select conditions appropriate for diffusion to dominate or use short exposure times. Optimal conditions for direct writing photopolymerization were identified and illustrated in Fig. 6D2 and D3, 7B and 8C1. Alternatively, to produce hollow cylinders of gels, one should employ conditions under which reaction dominates, illustrated in Fig. 6C5, 7C, and 8D3.

This model is incomplete in three major ways. First, the model is not predictive. The model assumes effective rate constants for the various stages of the polymerization process. In principle, these effective rate constants could be calculated from known elementary chemical mechanisms for which rate constants have been determined in order to construct a predictive theory of the photopolymerization process. Second, in our experiments, we focused on thin samples. As shown in Fig. 2, interesting behavior occurs for thick samples, which could be investigated more fully with experiments. Third, gelation is absent from the model.

Our numerical solution of the model, in which we assumed that all of the reaction constants and diffusion constants are equal, replicates the gross phenomenology observed experimentally. However, this correspondence between experiment and theory does not prove that the rate and diffusion constants are equal; rather, the correspondence between the model and the experiment suggests that there is a single rate limiting step, such as the polymerization rate, which controls the process. We note that there are some experimental features, such as the observation of a rapid growing wave of polymerization, illustrated in Video SII,† that are not captured by the model. Additional work is needed to determine if unequal reaction–diffusion coefficients in eqn (14) and/or the addition of new steps in the model are required to reconcile theory and experiment.

This paper presents the first report of the creation of non-uniform hydrogels using uniform illumination. Because photolithography of hydrogels is widespread, the question arises as to why the non-uniformity we report has not been previously observed. Our explanation is that previous studies were performed in the limit of either the diffusion constant, D, being small[1] or the exposure time, t, being short.[18]

The model makes non-trivial predictions. For example, to create a uniform gel, use short exposure times so that the chemical reactants do not have time to diffuse across the illumination zone, *e.g.* $\tau = 0.2$. As shown in Fig. 7(C4) this will result in a uniform gel but with low concentration of the polymer. To produce a higher density gel, increase the exposure time, but as shown in Fig. 7(C4) the resulting gel is non-uniform. This model predicts that repetitively cycling the illumination for a short period, *e.g.* $\tau = 0.2$, and then turning off the illumination for a time sufficient for the concentrations to become uniform again, *e.g.* $\tau = 2$ results in a dense and uniform gel.

5. Conclusion

Through the direct patterning method, it is possible to fabricate pNIPAAM gel structures on the length scale of tens of microns. We studied the variation of the size and uniformity of photopolymerized pNIPAAM microstructures as functions of experimentally controllable parameters and developed a reaction–diffusion model of the photopolymerization process. Through the comparison of experiment and theory, the effects of the exposure time, exposure intensity, monomer concentration, and terminator concentration were analyzed.

For exposure times greater than the time for a monomer to diffuse across the illuminated region ($\tau > 1$), uniform gels were produced under diffusion dominated conditions ($K \ll 1$), while hollow cylinders were produced under reaction dominated conditions ($K \gg 1$). Short exposure times ($\tau < 1$) always produce uniform gels. We observed a similar behavior in the hydrogel HEMA, which is a non-thermosensitive gel. As the model is general, we expect that these results will apply to many types of hydrogels structured on the micron scale with photopolymerization in addition to the pNIPAAM and HEMA gels studied here. Consequently, the considerations discussed here will guide the fabrication of microstructured hydrogels using photolithography or 3D printing for applications in the fields of microfluidics, microactuators, and tissue engineering.

Acknowledgements

This work was partially supported by the Pioneer Research Center Program through the National Research Foundation of Korea funded by the Ministry of Science, ICT & Future Planning (2009-0082954) and a grant from the National Science Foundation MRSEC (DMR-0820492). The authors would like to thank the Olin College 2009 and 2010 SCOPE Teams for the instrumentation of the motorized stages.

References

1 K. C. Hribar, P. Soman, J. Warner, P. Chung and S. Chen, *Lab Chip*, 2014, **14**, 268–275.
2 I. C. Kwon, Y. H. Bae and S. W. Kim, *Nature*, 1991, **354**, 291–293.
3 Q. Z. Luo, S. Mutlu, Y. B. Gianchandani, F. Svec and J. M. J. Frechet, *Electrophoresis*, 2003, **24**, 3694–3702.
4 K. Nishida, M. Yamato, Y. Hayashida, K. Watanabe, N. Maeda, H. Watanabe, K. Yamamoto, S. Nagai, A. Kikuchi, Y. Tano and T. Okano, *Transplantation*, 2004, **77**, 379–385.
5 D. Dendukuri, S. S. Gu, D. C. Pregibon, T. A. Hatton and P. S. Doyle, *Lab Chip*, 2007, **7**, 818–828.
6 D. C. Pregibon, M. Toner and P. S. Doyle, *Science*, 2007, **315**, 1393–1396.
7 T. R. Hoare and D. S. Kohane, *Polymer*, 2008, **49**, 1993–2007.
8 D. Dendukuri and P. S. Doyle, *Adv. Mater.*, 2009, **21**, 4071–4086.
9 M. E. Helgeson, S. C. Chapin and P. S. Doyle, *Curr. Opin. Colloid Interface Sci.*, 2011, **16**, 106–117.
10 K. W. Bong, J. J. Xu, J. H. Kim, S. C. Chapin, M. S. Strano, K. K. Gleason and P. S. Doyle, *Nat. Commun.*, 2012, 3.
11 A. Halperin and M. Kroeger, *Langmuir*, 2012, **28**, 16623–16637.
12 K. Nishida, M. Yamato, Y. Hayashida, K. Watanabe, K. Yamamoto, E. Adachi, S. Nagai, A. Kikuchi, N. Maeda, H. Watanabe, T. Okano and Y. Tano, *N. Engl. J. Med.*, 2004, **351**, 1187–1196.
13 D. Schmaljohann, J. Oswald, B. Jorgensen, M. Nitschke, D. Beyerlein and C. Werner, *Biomacromolecules*, 2003, **4**, 1733–1739.
14 L. Dong, A. K. Agarwal, D. J. Beebe and H. Jiang, *Nature*, 2006, **442**, 551–554.
15 D. Kim and D. J. Beebe, *Lab Chip*, 2007, **7**, 193–198.
16 S. B. Lee, D. I. Ha, S. K. Cho, S. J. Kim and Y. M. Lee, *J. Appl. Polym. Sci.*, 2004, **92**, 2612–2620.
17 X. Z. Zhang, D. Q. Wu and C. C. Chu, *Biomaterials*, 2004, **25**, 4719–4730.
18 D. Dendukuri, P. Panda, R. Haghgooie, J. M. Kim, T. A. Hatton and P. S. Doyle, *Macromolecules*, 2008, **41**, 8547–8556.
19 D. Singh, D. Kuckling, V. Choudhary, H. J. Adler and V. Koul, *Polym. Adv. Technol.*, 2006, **17**, 186–192.
20 K. H. Hong, Y. S. Jeon and J. H. Kim, *Macromol. Res.*, 2009, **17**, 26–30.
21 M. Hidaka and R. Yoshida, *J. Controlled Release*, 2011, **150**, 171–176.
22 R. Yoshida, *Colloid Polym. Sci.*, 2011, **289**, 475–487.
23 R. Yoshida and Y. Murase, *Colloids Surf., B*, 2012, **99**, 60–66.
24 J. Delgado, Y. Zhang, B. Xu and I. R. Epstein, *J. Phys. Chem. A*, 2011, **115**, 2208–2215.
25 A. M. Fuxman, K. B. McAuley and L. J. Schreiner, *Macromol. Theory Simul.*, 2003, **12**, 647–662.
26 A. Giz, H. Catalgil-Giz, A. Alb, J. L. Brousseau and W. F. Reed, *Macromolecules*, 2001, **34**, 1180–1191.
27 S. Kizilel, V. H. Perez-Luna and F. Teymour, *Macromol. Theory Simul.*, 2006, **15**, 686–700.
28 V. I. Koeva, S. Daneshvar, R. J. Senden, A. H. M. Imam, L. J. Schreiner and K. B. McAuley, *Macromol. Theory Simul.*, 2009, **18**, 495–510.